small methods
www.small-methods.com

Hierarchically Ordered Nanoporous Carbon with Exclusively Surface-Anchored Cobalt as Efficient Electrocatalyst

*Chaoyun Tang, Maricely Ramírez-Hernández, Belvin Thomas, Yao-Wen Yeh, Philip E. Batson, and Tewodros Asefa**

A hierarchically ordered porous carbon electrocatalyst with exclusively surface-anchored cobalt species, dubbed Co@HOPC, is synthesized from polyaniline and cobalt-functionalized silica microparticles templates, and its high electrocatalytic activity for the oxygen evolution reaction (OER) is demonstrated. The material requires a small potential (320 mV) to drive the reaction with a current density of 10 mA cm^{-2} and a small Tafel slope of 31.2 mV dec^{-1}. Moreover, Co@HOPC shows better catalytic activity for OER than in situ cobalt-doped and surface cobalt-loaded hierarchically ordered porous carbon materials synthesized by traditional methods. This is due to the abundant surface cobalt species present in Co@HOPC and the material's good electrical conductivity. This work provides a new strategy to utilize functionalized silica microparticles as templates to synthesize hierarchically ordered porous carbon materials with metal-rich surfaces and efficient electrocatalytic activities.

1. Introduction

3D, hierarchically ordered porous carbon (HOPC) materials with tunable and well-defined macropores and interconnected micropores and/or mesopores have received tremendous attention due to their many interesting properties and various applications.[1] Their excellent structural features, which include physically robust carbon skeletons, high surface areas, and good electrical conductivity, make them especially suitable for various electrochemical applications; e.g., as electrodes for batteries, fuel cells, and supercapacitors and as support materials for electrocatalysts of different reactions.[2]

Generally, HOPC materials are synthesized using hard templates such as polystyrene or silica nano-/microparticles.[3] In a typical synthetic procedure, monodisperse nano-/microparticles (templates) are self-assembled into 3D crystalline arrays by sedimentation, their interparticle spaces are infiltrated with carbon precursors with/without metals, the composite materials are dried and pyrolyzed, and the templates are removed.[4] Using this method, Sun et al., for example, made HOPC with single-atom cobalt species embedded in its structure and then showed its catalytic activities for the oxygen reduction reaction and the hydrogen evolution reaction.[5] Their work also provided a new synthetic strategy to structurally-controlled single-atom-site (SAS) catalysts. In another example, Jeong et al. synthesized N-doped HOPC materials containing N-coordinated single-atom nickel sites that exhibit electrocatalytic activity toward the CO_2 reduction reaction (CO_2RR).[6] They also showed that the structures of the HOPC materials, particularly their robust 3D porous frameworks, would provide large surface areas suited for electrocatalysis. However, most of the metallic atoms in the carbon materials produced by these previously reported synthetic strategies are embedded in the carbon skeletons and thus unable to participate in electrochemical reactions, which generally take place only at the solid/liquid interfaces.[7]

Herein, we report a simple synthetic method that produces electrocatalytically active HOPC material with exclusively surface-anchored metallic sites, dubbed M@HOPC. This is achieved using monodisperse silica spheres (MDSS) pretreated with metal ions as templates (**Scheme 1**). First, MDSS functionalized with Co(II) ions are synthesized, then dispersed in water, centrifuged, and dried. The spaces within the resulting colloidal crystal are then filled with polyaniline with in situ polymerization of aniline. The resulting polyaniline/MDSS composite material is then pyrolyzed, and the silica templates are etched with an alkaline solution. This gives M@HOPC with a high surface area, large amounts of pores, and exclusively surface-anchored/-exposed electroactive metallic sites. The material also possesses hierarchically ordered carbon skeletons that allow electrons to smoothly move through. As a result, the

C. Tang
Hoffmann Institute of Advanced Materials
Shenzhen Polytechnic
Shenzhen 518060, P. R. China
C. Tang, B. Thomas, T. Asefa
Department of Chemistry and Chemical Biology
Rutgers
The State University of New Jersey
Piscataway, NJ 08854, USA
E-mail: tasefa@chem.rutgers.edu
C. Tang, M. Ramírez-Hernández, T. Asefa
Department of Chemical and Biochemical Engineering
Rutgers
The State University of New Jersey
Piscataway, NJ 08854, USA
Y.-W. Yeh, P. E. Batson
Department of Physics and Astronomy
Rutgers
The State University of New Jersey
Piscataway, NJ 08854, USA

The ORCID identification number(s) for the author(s) of this article can be found under https://doi.org/10.1002/smtd.202200519.

DOI: 10.1002/smtd.202200519

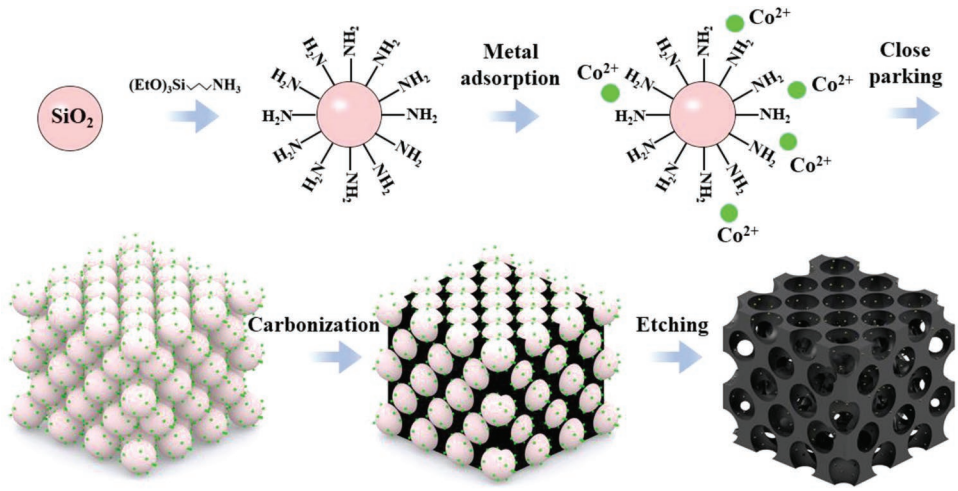

Scheme 1. Schematic illustration of the synthetic procedure used to produce exclusively surface-anchored metal (cobalt) on hierarchically ordered porous carbon (Co@HOPC). The material can serve as an efficient electrocatalyst for the oxygen evolution reaction (OER).

material can robustly drive the electrocatalytic oxygen evolution reaction (OER). While Co is chosen to demonstrate this, as a proof-of-concept, the synthetic method reported here should apply to other metals such as Fe and Ni, offering new opportunities for silica templates-assisted synthesis of efficient, sustainable electrocatalysts for various reactions.

2. Results and Discussions

2.1. Synthesis and Characterizations

To produce HOPC with metal-rich surfaces (Scheme 1), MDSS functionalized with amine groups, followed by metal ions, are synthesized via a method that we described previously.[8] These metal-functionalized MDSS are then used as hard templates for polymers (see details in the Experimental Section in the Supporting Information). Importantly, besides serving as templates, these nanoparticles are proven to enable the deployment of target metal ions exclusively onto the surfaces of the porous carbon materials derived from the polymers via pyrolysis. For a proof-of-concept study, Co(II) ions are chosen and used in this work. The Co(II) ions-functionalized MDSS (MDSS-Co) in aqueous solution are closely packed into colloidal crystals via centrifugation. Inside the interparticle pores of the dried colloidal crystal, polyaniline is grown via polymerization of aniline in situ. After pyrolysis of the resulting polyaniline/MDSS-Co at 900 °C in an inert atmosphere and then etching away the silica from the carbonized product with NaOH solution, Co@HOPC is obtained. To elucidate the effect of the material's structure on its electrocatalytic properties for OER, two control materials are synthesized and used as references. They include: i) cobalt-loaded HOPC, denoted Co/HOPC, that is synthesized by directly loading Co(II) ions onto as-synthesized metal-free HOPC;[9] and ii) in-situ cobalt-doped HOPC, named Co-HOPC, that is synthesized via a traditional method by using nonfunctionalized MDSS as templates (see the synthetic details provided in the Supporting Information).

These three Co-containing HOPC materials (i.e., Co@HOPC, Co/HOPC, and Co-HOPC) as well as the metal-free HOPC are characterized by various methods. Their X-ray diffraction (XRD) patterns (Figure S1, Supporting Information) are similar and show a peak at 26°, which is typical of carbon materials or other HOPC materials reported previously.[10] Furthermore, in all XRD patterns, no peaks associated with Co are observed. Since the presence of Co in these Co-containing HOPC materials is revealed by other methods (see below), the absence of XRD peaks associated with Co in the case of Co/HOPC and Co-HOPC must be because the cobalt species in the Co-containing HOPC materials are too small in amount or amorphous to diffract X-rays. In the case of Co@HOPC, it must be because the Co species are largely in the form of single atoms, as revealed by high-resolution electron microscopy image analyses below.

The materials also show similar decomposition patterns and nearly similar amounts of residues on their thermogravimetric analysis (TGA) curves (Figure S2, Supporting Information). More specifically, Co@HOPC, Co/HOPC, and Co-HOPC leave 1.26%, 2.30%, and 1.39% residues at 800 °C, respectively. The amounts of cobalt in the materials, determined by inductively coupled plasma optical emission spectroscopy (ICP-OES), are 1.096%, 1.092%, and 1.115%, respectively. As these values are very close to one another, the electrochemical properties of the three materials are compared with one another without normalizing them for the amounts of metals in them (vide infra). Raman spectra of all materials (Figure S3, Supporting Information) show bands at 1340 and 1580 cm^{-1} due to the typical D and G stretching modes of carbon structures, respectively. The peaks observed at 465 and 668 cm^{-1} on the Raman spectrum of Co/HOPC can be ascribed to the E_g and A_{1g} peaks of Co_3O_4, respectively,[11] and they indicate the existence of Co_3O_4 on the surfaces of this material.

The HOPC materials are then characterized by electron microscopy and associated techniques (**Figures 1** and **2**; and Figures S4–S6, Supporting Information). Their scanning electron microscopy (SEM) images show similar inverse opal and

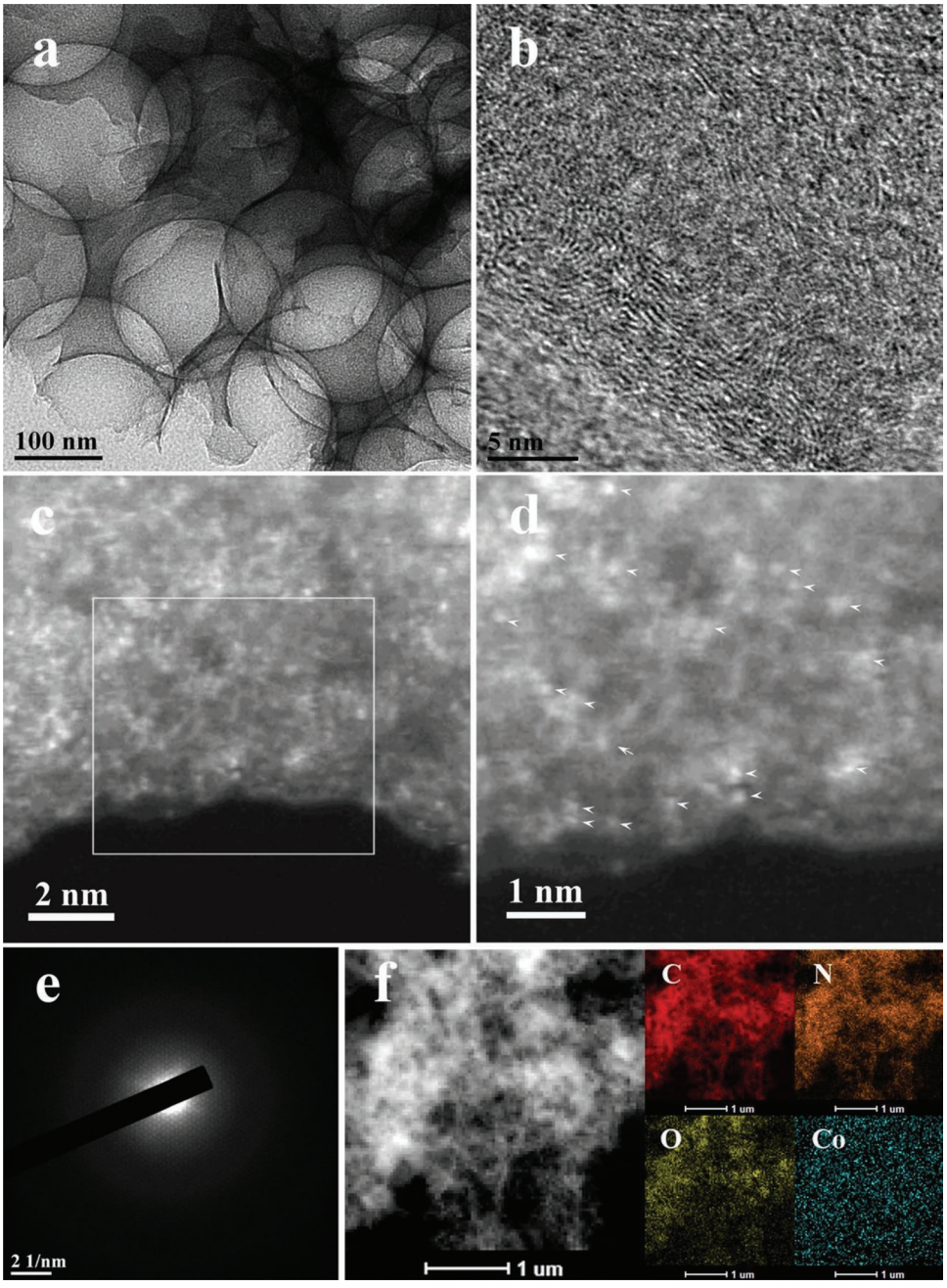

Figure 1. a,b) HRTEM images, c,d) HAADF-STEM images (with single Co atoms being highlighted with arrows), e) SAED pattern, and f) EDS elemental mapping images of Co@HOPC.

hierarchically nanoporous structures (Figure 1a; and Figure S4, Supporting Information). High-resolution transmission electron microscope (HRTEM) images of Co/HOPC reveal that this material possesses nanoparticles with a dimension of 20–50 nm (Figure S5a, Supporting Information). Representative HRTEM image of these nanoparticles shows lattice fringes with an interplanar spacing of 0.243 nm (Figure S5b, Supporting Information), which corresponds to the (311) plane of Co_3O_4. Selected area electron diffraction (SAED) pattern of Co/HOPC (Figure S5c, Supporting Information) exhibits distinct diffraction spots corresponding to the characteristic (111), (200), (400), and (311) planes of Co_3O_4. Representative elemental mapping images of all three materials, obtained with a high-resolution energy-dispersive X-ray spectrometer (EDS) (Figure 1f; and Figures S5d and S6d, Supporting Information), show well-distributed C and N atoms, which must be due to the N-doped carbon structures in them that are derived from polyaniline.[12] The images for Co/HOPC (Figure S5d, Supporting Information) show O and Co, which must be due to the Co_3O_4 nanoparticles formed in this material.

Representative elemental mapping images of Co@HOPC (Figure 1f) and Co-HOPC (Figure S6d, Supporting Information)

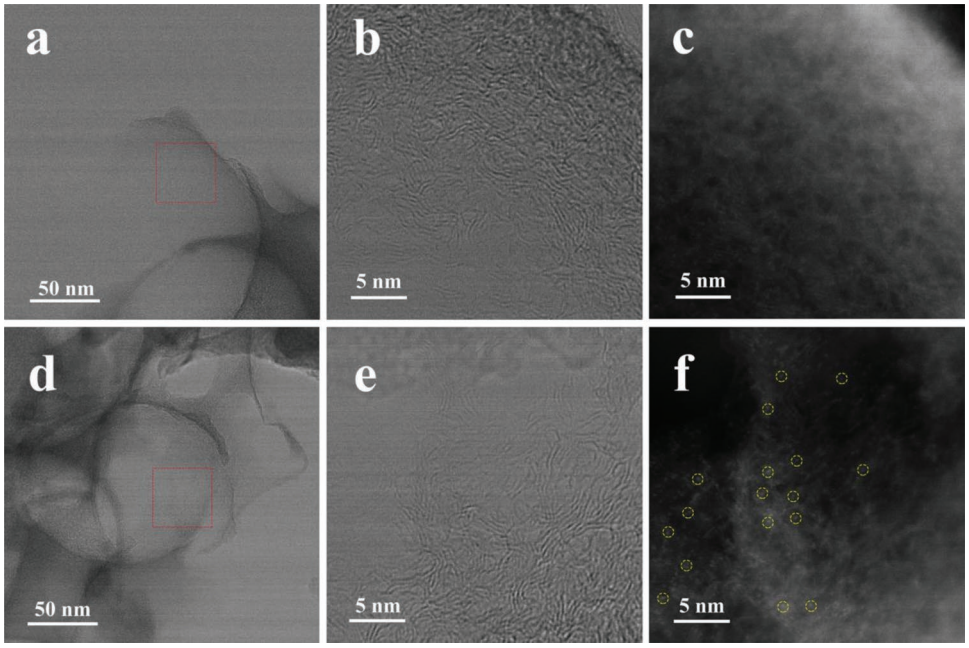

Figure 2. Comparison of the HRTEM and HAADF-STEM images of a–c) Co-HOPC versus d–f) Co@HOPC, with single Co atoms shown with circles in the image displayed in (f).

also show well-distributed C, N, O, and Co. This indicates that the in situ doping and exclusively surface-anchoring synthetic methods lead to well-distributed Co species on the carbon materials. Meanwhile, the HRTEM images of these two HOPC materials (Figures 1a,b and 2; and Figure S7, Supporting Information) show no obvious lattice fringes associated with Co, and their SAED images (Figure 1e and Figure S6c, Supporting Information) show no diffraction patterns. However, single Co atoms are observed in HAADF-STEM images (Figures 1c,d and 2f). Furthermore, the images for Co@HOPC clearly show much more surface Co atoms compared with Co-HOPC (Figure 2c,f), proving that the surface atom-anchoring synthetic strategy is successful and that it offers the advantage of placing lots of surface exposed Co atoms on nanoporous carbon nanomaterials. The density of single Co atoms Co@HOPC is found to be ≈5 Co atoms nm^{-2} (Figure S7, Supporting Information).

The Brunauer–Emmett–Teller (BET) surface areas of metal-free and cobalt-containing HOPC materials are determined using the adsorption/desorption isotherms obtained for them using N_2 porosimetry (Figure S8a, Supporting Information). The BET surface areas of Co@HOPC, Co/HOPC, and Co-HOPC are 491, 450, and 468 $m^2\ g^{-1}$, respectively. These values are a little higher than that of metal-free HOPC (444 $m^2\ g^{-1}$) and those of other metal-free HOPC materials previously reported.[13a] The pore size distributions of the materials, which are determined by the Barrett–Joyner–Halenda (BJH) method (Figure S8b, Supporting Information), appear similar. Notably, their pores range between 7 and 30 nm, with the average values being centered at around 16 nm, in all of them. Their similar pore structures are not surprising as they are all made using similar types of silica nanoparticles as templates.

The composition, electronic states, and nature of bonding of the elements in the three cobalt containing HOPC materials are investigated using X-ray photoelectron spectroscopy (XPS) (**Figure 3**). The survey XPS spectra of the materials show peaks corresponding to Co, C, N, and O (Figure S9, Supporting Information). Their C 1s core-level XPS spectra (Figure 3a) exhibit similar peaks at ≈284.6 and 285.8 eV, which are attributable to C—C and C—N/C—O species, respectively. Their XPS spectra of N 1s core level (Figure 3b) show peaks at ≈398.3 and 400.9 eV, which are associated with the pyridinic and quaternary N atoms, respectively, of N dopants in the polyaniline-derived N-doped carbon structures of HOPC. The XPS peak at 530.4 eV, which is associated with O 2p of Co-O species, is relatively more intense for Co/HOPC compared with those of Co-HOPC and Co@HOPC (Figure 3c). The XPS spectrum of Co/HOPC (Figure 3d) also shows peaks at ≈780.7 eV, which can be ascribed to Co^{2+} and Co^{3+} species.[14] Otherwise, the spectra of the three HOPC materials display similar peaks, indicating their predominantly similar surface compositions.

2.2. Electrochemical Performances

To study the electrocatalytic properties of the HOPC materials toward OER, first, each material is uniformly deposited onto a glassy carbon electrode (GCE), with a catalyst loading of 0.2 mg cm^{-2}. By using the prepared electrodes as working electrodes, linear sweep voltammetry (LSV) curves are recorded in O_2-saturated KOH solution (1 M). For comparison, similar curves are obtained for working electrodes comprising metal-free HOPC and commercial RuO_2 catalysts that are deposited on GCE. Before the comparison is made, the ohmic potential (*iR*) drop due to the resistance of the electrolyte is compensated in each measurement. The LSV curves (**Figure 4**a) show that, compared with metal-free HOPC, all three cobalt-containing HOPC materials exhibit better electrocatalytic activities for OER by requiring smaller overpotentials to drive the reaction.

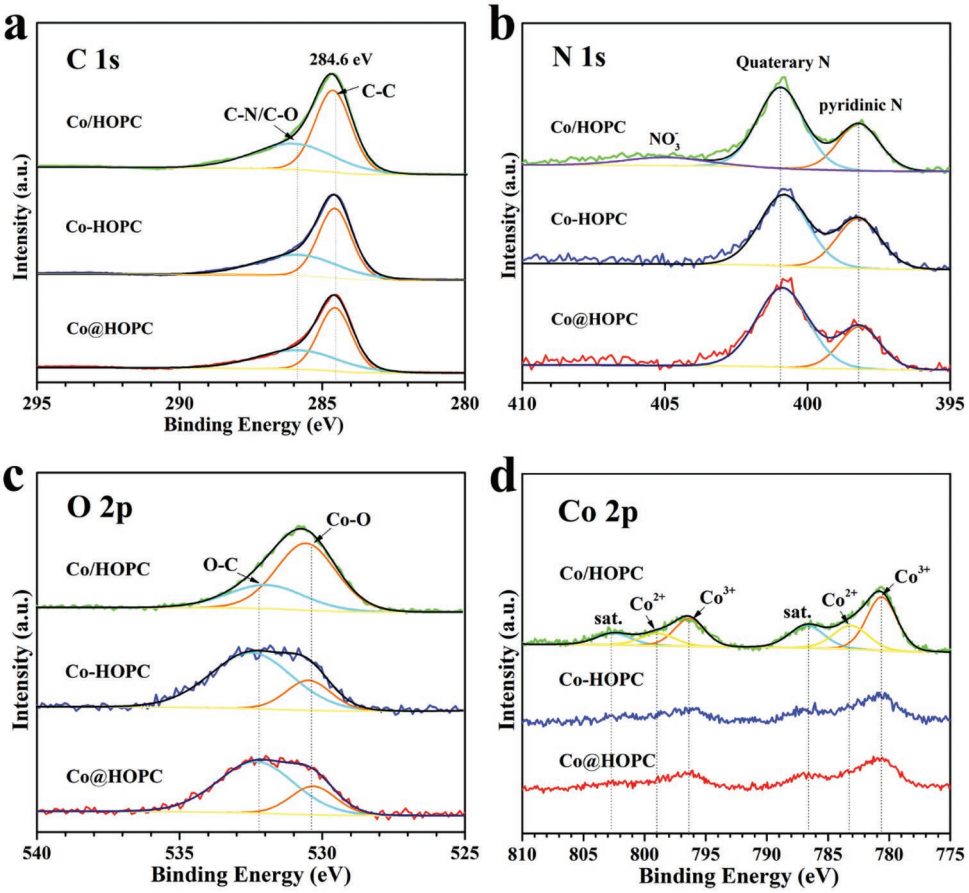

Figure 3. XPS spectra of the three cobalt containing HOPC materials (Co/HOPC, Co-HOPC, and Co@HOPC), showing their a) C 1s, b) N 1s, c) O 2p, and d) Co 2p peaks.

This indicates that cobalt constitutes the actual catalytic sites in these cobalt-containing HOPC materials, just like other Co-based electrocatalysts reported previously.[15] Among the HOPC materials, Co@HOPC shows the best electrocatalytic activity by driving the reaction at a current density of 10 mV cm^{-2} (η_{10}) with an overpotential of 320 mV. Notably also, the electrocatalytic activities of Co@HOPC and Co-HOPC are better than that of RuO_2, the benchmark OER catalyst.

Tafel plots are obtained for the reactions over the materials to evaluate the kinetics of the catalytic processes in each case (Figure 4b). The Tafel slope for Co@HOPC (31.2 mV dec^{-1}) is lower than those of Co-HOPC (56.1 mV dec^{-1}), Co/HOPC (86.7 mV dec^{-1}), and RuO_2 (85.0 mV dec^{-1}). This indicates that the kinetics of OER over Co@HOPC is more favorable than those over the other materials, including RuO_2. It is worth adding here that Co@HOPC catalyzes the

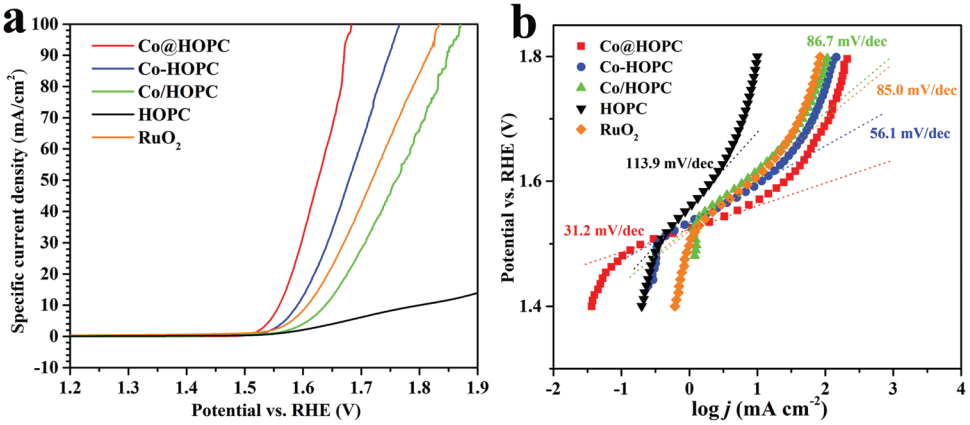

Figure 4. a) Linear sweep voltammetry (LSV) curves and b) the corresponding Tafel plots of OER over Co-containing HOPC materials in 1 M KOH solution.

reaction with a smaller Tafel slope than Co-HOPC and Co/HOPC do, even though all three have nearly similar amounts of Co. This may have been partly contributed by the differences in the resistances of the materials or their abilities to transfer charges on their surfaces, which are known to affect the Tafel slope.[18] The Tafel slope can also be used to identify the rate-limiting electron-/proton-transfer steps in the OER.[16] For example, the Tafel slope of 31.2 mV dec^{-1} obtained for Co@HOPC indicates that the second/third electron transfer step in the reaction over this material is the rate-determining step.[17] Based on the Tafel slopes, Co@HOPC can be said to be the most efficient OER electrocatalyst among the three HOPC materials investigated. It is also among the best Co-based OER electrocatalysts compared with several related materials reported in the literature (Table S1, Supporting Information).[19]

Next, the conductivity of the HOPC materials and the kinetics of the reaction over them under OER conditions are studied via electrochemical impedance spectroscopy (EIS). Their Nyquist plots (**Figure 5**a) reveal that Co@HOPC has a charge-transfer resistance (R_{ct}) of 8.4 Ω, which is close to those of Co/HOPC (8.8 Ω) and metal-free HOPC (9.2 Ω). This is indicative of their similar underlying conductive carbon structures. However, Co-HOPC shows a relatively larger value of R_{ct} (12.6 Ω), indicating that the cobalt species embedded in its carbon skeleton somehow compromise its conductivity. This difference in the values of R_{ct} between some of these Co-containing HOPC materials could partly account for the difference in their electrocatalytic activities.

Mechanistic studies of OER over catalysts containing transition metals (such as Ni and Co) in alkaline electrolytes have been proposed to involve a preactivation step (step 1) and three consecutive elementary steps (steps 2–4) that are shown for Co below[20]

$$Co^{2+} + 3OH^- \rightleftharpoons CoOOH + H_2O + e^- \quad (1)$$

$$CoOOH + OH^- \rightleftharpoons CoO(OH)_2 + e^- \quad (2)$$

$$CoO(OH)_2 + 2OH^- \rightleftharpoons CoOO_2 + 2H_2O + 2e^- \quad (3)$$

$$CoOO_2 + OH^- \rightarrow CoOOH + O_2 + e^- \quad (4)$$

$$\text{Net Reaction of OER } (2-4): 4OH^- \rightarrow O_2 + 2H_2O + 4e^- \quad (5)$$

Steps 1, 2, and 3 are reversible and determine the overall rate of reaction, whereas step 4 is fast and irreversible. The OER on the Co-containing HOPC catalysts is expected to follow a similar mechanism as those on other Co-based OER electrocatalysts reported previously.[18] In the process, the cobalt atoms on the surfaces of the catalysts are partially oxidized to CoOOH, with some of the CoOOH species further going to $CoOO_2$ at a higher potential, to be followed by O_2 evolution and CoOOH regeneration.[21] Therefore, the amount of surface cobalt species that can undergo these redox reactions crucially dictates the electrochemically active surface area (ECSA) of such catalysts.

To assess this, the electrochemical double-layer capacitances (C_{dl}), which is directly correlated to ECSA, of the HOPC materials are determined, and the values are compared among one another (Figure 5b). The value for Co@HOPC (6.9 mF cm^{-2}) is much bigger than those of Co-HOPC (1.02 mF cm^{-2}), Co/HOPC (0.569 mF cm^{-2}), and metal-free HOPC (0.181 mF cm^{-2}). These results indicate the presence of an abundant amount of cobalt on the surfaces of Co@HOPC. It also indicates the accessibility as well as the participation of these Co species as catalysts in the electrochemical redox reaction at the solid/liquid interfaces of the materials. After being normalized by ECSA, the current densities of OER over Co@HOPC and Co-HOPC are found to be similar though (Figure S10, Supporting Information), suggesting the surface Co species in both materials have similar intrinsic electrocatalytic activities for the reaction. Therefore, the higher electrocatalytic performance of Co@HOPC toward OER is mainly due to be its exceptional large amount of surface Co species.

Finally, the stability of the three electrocatalysts during OER is assessed for 24 h with chronoamperometry at the respective potentials that drive OER over the catalysts at j = 10 mA cm^{-2} (Figure 5c). The current density for Co/HOPC decreases during the first 2 h, but then becomes stable, suggesting that the surface cobalt species on this material are compromised or etched during the first 2 h of OER.[22] The overall decrease in current density of OER over Co/HOPC in 24 h is 20%. The one on Co-HOPC and Co@HOPC is more stable, showing an overall decrease in current density of 12% in 24 h. The losses in activity

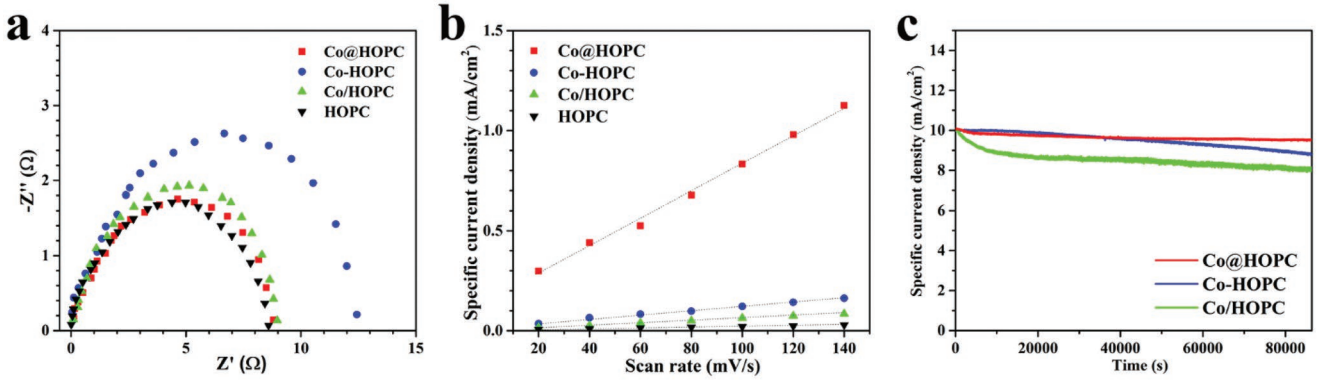

Figure 5. a) Electrochemical impedance spectra (EIS) obtained at an overpotential of 300 mV and b) measured capacitive current versus scan rate for OER over different HOPC materials. c) Current density versus time (*i*–*t*) profiles for the OER over of three cobalt-containing HOPC materials at a potential corresponding to j = 10 mA cm^{-2} in 1 M KOH solution for 24 h.

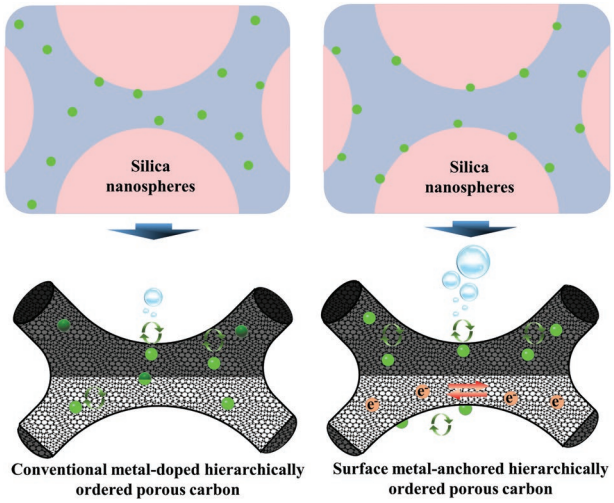

Figure 6. Schematic illustration of the differences in structures, and thus OER electrocatalytic activities, between Co@HOPC (HOPC with exclusively surface-anchored Co species) and Co-HOPC (HOPC possessing Co embedded in its carbon frameworks).

for these two HOPC materials are similar to those of some previously reported Co-based SAS catalysts.[23] Interestingly, the current density of the reaction over Co@HOPC shows barely any loss, corroborating this material's superior stability and durability as an electrocatalyst for OER.

The stability and efficient OER electrocatalytic properties activities of Co@HOPC, compared with those of Co-HOPC and Co/HOPC, can be attributed to its two unique structural features, as illustrated in **Figure 6**. i) Co@HOPC possesses cobalt species exclusively on its surfaces that can participate as catalytic sites in an electrochemical reaction, without compromising charge and mass transfer kinetics in the material (whereas Co-HOPC possesses cobalt species that are mostly embedded within the carbon skeleton and are thus inaccessible). ii) The intact hierarchically ordered carbon framework of Co@HOPC guarantees electron transfer within its structures, whereas the in situ embedded Co in Co-HOPC inhibits electron transfer pathways or increases the charge-transfer resistance in the material. Meanwhile, the Co species in Co/HOPC are unstable during the reaction.

3. Conclusions

In summary, we have developed a synthetic route to hierarchically ordered porous carbon framework containing exclusively surface-anchored metal or Co-species (Co@HOPC) that can serve as an efficient electrocatalyst for the OER. Because of its unique structures, which includes surface abundant single Co atoms and inherent electrical conductivity, the as-synthesized Co@HOPC exhibited a higher electrocatalytic activity for the reaction compared with in situ Co-doped and surface Co-loaded HOPC materials that are synthesized via conventional synthetic methods. The former could electrocatalyze OER at a current density of 10 mA cm^{-2} with a smaller potential of 320 mV and a smaller Tafel slope of 31.2 mV dec^{-1}. This work paves a new route for designing and synthesizing highly efficient and sustainable OER electrocatalysts composed of hierarchically ordered carbon structures by using surface-modified monodisperse silica nanoparticles as templates for various renewable energy conversion and storage devices.

Supporting Information

Supporting Information is available from the Wiley Online Library or from the author.

Acknowledgements

C.T. acknowledges the financial support from Post-doctoral Later-stage Foundation Project of Shenzhen Polytechnic (No. 6019211006K).

Conflict of Interest

The authors declare no conflict of interest.

Data Availability Statement

The data that support the findings of this study are available from the corresponding author upon reasonable request.

Keywords

cobalt catalysts, electrocatalysis, hierarchically ordered nanoporous carbon, oxygen evolution reaction, silica templates

Received: April 21, 2022
Published online:

[1] a) C. Vix-Guterl, E. Frackowiak, K. Jurewicz, M. Friebe, J. Parmentier, F. Béguin, *Carbon* **2005**, *43*, 1293; b) S. Zhang, L. Chen, S. Zhou, D. Zhao, L. Wu, *Chem. Mater.* **2010**, *22*, 3433; c) J. Wang, J. Kim, S. Choi, H. Wang, J. Lim, *Small Methods* **2020**, *4*, 2000621.
[2] a) S. Dutta, A. Bhaumik, K. C. W. Wu, *Energy Environ. Sci.* **2014**, *7*, 3574; b) Y. Wang, S. Luo, M. Chen, L. Wu, *Adv. Funct. Mater.* **2020**, *30*, 2000373; c) J. Gu, S. Magagula, J. Zhao, Z. Chen, *Small Methods* **2019**, *3*, 1800550.
[3] M. Liu, X. Xiao, Q. Li, L. Luo, M. Ding, B. Zhang, Y. Li, J. Zou, B. Jiang, *J. Colloid Interface Sci.* **2022**, *607*, 791.
[4] J. Cui, Q. Chen, X. Li, S. Zhang, *Green Chem.* **2021**, *23*, 6898.
[5] T. Sun, S. Zhao, W. Chen, D. Zhai, J. Dong, Y. Wang, S. Zhang, A. Han, L. Gu, R. Yu, X. Wen, H. Ren, L. Xu, C. Chen, Q. Peng, D. Wang, Y. Li, *Proc. Natl. Acad. Sci. USA* **2018**, *115*, 12692.
[6] H.-Y. Jeong, M. Balamurugan, V. S. K. Choutipalli, E.-s. Jeong, V. Subramanian, U. Sim, K. T. Nam, *J. Mater. Chem. A* **2019**, *7*, 10651.
[7] a) C. Zhu, Q. Shi, S. Feng, D. Du, Y. Lin, *ACS Energy Lett.* **2018**, *3*, 1713; b) J. Zhang, C. Dong, Z. Wang, H. Gao, J. Niu, Z. Peng, Z. Zhang, *Small Methods* **2019**, *3*, 1800286.
[8] Y. Wang, A. V. Biradar, C. T. Duncan, T. Asefa, *J. Mater. Chem.* **2010**, *20*, 7834.

[9] T. Zhang, T. Asefa, *Front. Chem. Sci. Eng.* **2018**, *12*, 329.
[10] T.-C. Chou, C.-H. Huang, R.-A. Doong, C.-C. Hu, *J. Mater. Chem. A* **2013**, *1*, 2886.
[11] a) A. Diallo, A. Beye, T. Doyle, E.-S. Park, M. Maaza, *Green Chem. Lett. Rev.* **2015**, *8*, 30; b) S. Farhadi, M. Javanmard, G. Nadri, *Acta Chim. Slov.* **2016**, *63*, 335.
[12] R. Silva, D. Voiry, M. Chhowalla, T. Asefa, *J. Am. Chem. Soc.* **2013**, *135*, 7823.
[13] a) J. Chen, S. He, B. Huang, P. Wu, Z. Qiao, J. Wang, L. Zhang, G. Yang, H. Huang, *ACS Appl. Mater. Interfaces* **2017**, *9*, 10684; b) J. Feng, D. Zheng, X. Gao, W. Que, W. Shi, W. Liu, F. Wu, X. Cao, *Front. Energy Res.* **2020**, *8*, 210.
[14] a) K. Shen, L. Zhang, X. Chen, L. Liu, D. Zhang, Y. Han, J. Chen, J. Long, R. Luque, Y. Li, B. Chen, *Science* **2018**, *359*, 206; b) X. Dai, Y. Dai, J. Lu, L. Pu, W. Wang, J. Jin, F. Ma, N. Tie, *Ionics* **2020**, *26*, 2501.
[15] a) L. Cao, Q. Luo, W. Liu, Y. Lin, X. Liu, Y. Cao, W. Zhang, Y. Wu, J. Yang, T. Yao, S. Wei, *Nat. Catal.* **2019**, *2*, 134; b) X. Li, P. Cui, W. Zhong, J. Li, X. Wang, Z. Wang, J. Jiang, *Chem. Commun.* **2016**, *52*, 13233.
[16] R. L. Doyle, I. J. Godwin, M. P. Brandon, M. E. G. Lyons, *Phys. Chem. Chem. Phys.* **2013**, *15*, 13737.
[17] M. S. Burke, M. G. Kast, L. Trotochaud, A. M. Smith, S. W. Boettcher, *J. Am. Chem. Soc.* **2015**, *137*, 3638.
[18] K. Xu, P. Chen, X. Li, Y. Tong, H. Ding, X. Wu, W. Chu, Z. Peng, C. Wu, Y. Xie, *J. Am. Chem. Soc.* **2015**, *137*, 4119.
[19] a) W. H. Lee, Y.-J. Ko, J.-Y. Kim, B. K. Min, Y. J. Hwang, H.-S. Oh, *Chem. Commun.* **2020**, *56*, 12687; b) X. Lv, W. Wei, H. Wang, B. Huang, Y. Dai, *Appl. Catal. B* **2020**, *264*, 118521; c) X. Zhong, W. Yi, Y. Qu, L. Zhang, H. Bai, Y. Zhu, J. Wan, S. Chen, M. Yang, L. Huang, M. Gu, H. Pan, B. Xu, *Appl. Catal. B* **2020**, *260*, 118188; d) X. Sun, S. Sun, S. Gu, Z. Liang, J. Zhang, Y. Yang, Z. Deng, P. Wei, J. Peng, Y. Xu, C. Fang, Q. Li, J. Han, Z. Jiang, Y. Huang, *Nano Energy* **2019**, *61*, 245; e) S. Dilpazir, H. He, Z. Li, M. Wang, P. Lu, R. Liu, Z. Xie, D. Gao, G. Zhang, *ACS Appl. Energy Mater.* **2018**, *1*, 3283.
[20] K. Juodkazis, J. Juodkazytė, R. Vilkauskaitė, V. Jasulaitienė, *J. Solid State Electrochem.* **2008**, *12*, 1469.
[21] S. Fu, C. Zhu, J. Song, M. H. Engelhard, X. Li, D. Du, Y. Lin, *ACS Energy Lett.* **2016**, *1*, 792.
[22] Z. Li, Z. Wang, S. Xi, X. Zhao, T. Sun, J. Li, W. Yu, H. Xu, T. S. Herng, X. Hai, P. Lyu, M. Zhao, S. J. Pennycook, J. Ding, H. Xiao, J. Lu, *ACS Nano* **2021**, *15*, 7105.
[23] Q. Zhang, Z. Duan, M. Li, J. Guan, *Chem. Commun.* **2020**, *56*, 794.